RSC Advances

PAPER

View Article Online
View Journal | View Issue

Cite this: *RSC Adv.*, 2026, **16**, 4032

Effects of graphene oxide incorporation *via* non-covalent interfacial interactions on the properties of small intestinal submucosa

Mianshu Hu, [a] Xiuyun Chuan,*[a] Yiting Wang,*[b] Wenyue Cheng,[c] Yun Yan, [d] Wenbin Zhang, [d] Kun Zhang,[b] Jinsong Han[b] and Jian Zhang[c]

To investigate the modifying effect of graphene oxide (GO) on small intestinal submucosa (SIS), GO-SIS biocomposite films were fabricated *via* a non-covalent coating strategy. Structural analyses confirmed the non-covalent interactions between GO and SIS collagen fibers and the preservation of SIS's native fibrous structure. The GO-SIS biocomposite film showed significantly improved hydrophilicity (contact angle: 71.3 ± 1.0°, $p < 0.001$; water absorption: 159.00 ± 5.60%, $p < 0.01$) compared to the SIS film. It also exhibited superior mechanical properties under both dry and wet conditions, with significantly higher tensile strength (dry: 24.46 ± 0.99 MPa; wet: 10.16 ± 0.37 MPa) and elongation at break (dry: 11.41 ± 0.55%; wet: 21.26 ± 0.65%) than the SIS film ($p < 0.001$ for all comparisons). After *in vitro* degradation, the GO-SIS biocomposite film showed better morphological stability compared to the SIS film. At 4, 8, 16, 24, 48, and 72 hours, the *in vitro* degradation of the GO-SIS biocomposite film was significantly slower than that of the SIS film. Furthermore, at 4, 8, 16, and 24 hours, the tensile strength and elongation at break of the degraded GO-SIS biocomposite film were significantly higher than those of the degraded SIS film. Biocompatibility assessment indicated no impact on L929 fibroblast viability or proliferation, along with favorable hemocompatibility. Collectively, the non-covalent incorporation of GO effectively enhances the hydrophilicity and mechanical performance of the GO-SIS biocomposite film and slows down its *in vitro* degradation, offering a promising strategy for the design of advanced tissue repair materials.

Received 2nd December 2025
Accepted 13th January 2026

DOI: 10.1039/d5ra09329e

rsc.li/rsc-advances

1. Introduction

Small intestinal submucosa (SIS) is an excellent natural extracellular matrix (ECM) material with a porous three-dimensional (3D) structure, processed *via* decellularization.[1–3] SIS is primarily composed of type I and III collagen fibers, with small amounts of type IV and V collagen, and preserves various bioactive factors.[3–5] Owing to its collagen fiber structure, excellent biocompatibility, low immunogenicity, and resorbability, SIS has attracted widespread interest in the field of tissue repair.[1,6,7] However, its clinical application is limited by rapid degradation and poor long-term mechanical support.[6,8] Therefore, modifications of SIS are desired to address these shortcomings.[4,8–11] Cao *et al.*[8] combined chitosan (CS)/elastin (ES) electrospun nanofibers with SIS, improving its biodegradability and antimicrobial activity. Tang *et al.*[9] designed a composite patch by *in situ* solidification of viscous polyvinyl alcohol (PVA) solution on the SIS surface, which provided dynamic mechanical support.

Graphene oxide (GO) has attracted considerable attention in the biomedical field. As an important derivative of graphene, GO retains the large planar structure of graphene, while carboxyl (–COOH) groups are introduced at the edges, and hydroxyl (–OH) and epoxy (C–O–C) groups are incorporated on the basal plane.[12,13] Due to its excellent properties, such as mechanical performance,[14,15] electrochemical properties,[16–18] optical performance,[19,20] amphiphilicity,[21] antimicrobial and antiviral activities,[22,23] biocompatibility,[24,25] and biodegradability,[26,27] many researchers have considered applying GO and its polymers to tissue engineering. Li *et al.*[28] developed a polydopamine-mediated graphene oxide (PGO)-hydroxyapatite (PHA)-alginate/gelatin (AG) composite scaffold, which exhibited excellent electrical conductivity and immunomodulatory ability, facilitating the repair and regeneration of periodontal bone tissue. Heidari *et al.*[29] fabricated poly(ε-caprolactone) (PCL)/gelatin/GO electrospun scaffolds, where the incorporation of GO resulted in outstanding antibacterial properties. Wan *et al.*[30] produced PCL-GO nanofiber membranes *via*

[a]*Key Laboratory of Orogenic Belts and Crustal Evolution, School of Earth and Space Sciences, Peking University, Beijing 100871, China. E-mail: xychuan@pku.edu.cn; bysywangyiting@126.com*

[b]*Peking University Third Hospital, Beijing 100191, China*

[c]*Naval Medical University, Shanghai Changzheng Hospital, Shanghai 200003, China*

[d]*College of Chemistry and Molecular Engineering, Peking University, Beijing 100871, China*

electrospinning, reporting that the addition of GO nanosheets significantly enhanced the mechanical properties and bioactivity of the PCL membrane. In another study, Cifuentes *et al.*[31] prepared a SIS-reduced graphene oxide (rGO) scaffold by mixing dissolved SIS powder with a GO dispersion, followed by freeze-drying and reduction. The results confirmed that the presence of GO or rGO did not compromise the scaffold's excellent biocompatibility, highlighting their potential for tissue engineering applications.

Based on the above, we aim to combine the natural structural advantages of intact SIS with the enhanced functionalities of GO. Therefore, we can avoid using methods such as electrospinning or freeze-drying to mimic the collagen fiber structure of SIS. Moreover, compared to covalent modifications, non-covalent approaches generally avoid harsh chemical reactions, simplify the preparation process, and prevent the introduction of potentially harmful chemical groups.[32] It has been reported that non-covalent interfacial interactions (such as electrostatic interactions and hydrogen bonding) exist between GO and collagen.[12,33–35] These strong non-covalent interactions not only enable GO to guide the self-assembly of collagen molecules but also enhance the mechanical properties and biocompatibility of GO/collagen composites.[34,35]

Therefore, we propose introducing GO into the SIS matrix *via* a coating method based on non-covalent interactions. This approach aims to develop a composite with enhanced hydrophilicity, mechanical properties and slower *in vitro* degradation, while leveraging and preserving the inherent advantages of SIS.

In this study, GO dispersions were coated onto single-layer SIS films, and GO-SIS biocomposite films were subsequently prepared *via* vacuum drying. The effects of GO incorporation and the non-covalent interfacial interactions between GO and SIS on the hydrophilicity, mechanical properties, *in vitro* degradation behavior, and biocompatibility of the composite films were investigated.

2. Experimental

2.1. Materials

Graphene oxide (GO) dispersion (SE3522, solid content 1.0%, D50 $\leq$ 4 μm) was purchased from Sixth Element (Changzhou) Materials Technology Co., Ltd (Changzhou, China). According to the supplier's datasheet, the GO was synthesized *via* the Hummers' method,[36] and exhibits a high oxidation degree. A single-layer small intestinal submucosa (SIS) film (5 cm × 15 cm) was used as the base material, supplied by Zhuo Ruan Medical Technology Co., Ltd (Suzhou, China) as a decellularized, sterilized, ready-to-use dry film. Phosphate buffer saline (PBS, 0.01 M, pH 7.4) was purchased from Beijing Labgic Technology Co., Ltd (Beijing, China). Collagenase I (C0130) was purchased from Sigma-Aldrich (Shanghai) Trading Co., Ltd (Shanghai, China). Hydroxyproline (Hyp) content assay kit (BC0250) was purchased from Beijing Solarbio Science & Technology Co., Ltd (Beijing, China). L929 fibroblasts (iCell-m026) and the recommended culture medium (iCell-m026-001b) were purchased from iCell Bioscience Inc (Shanghai, China). The cell counting kit-8 (CCK-8, HY-K0301) was purchased from MedChemExpress, USA. The live/dead double staining kit (Calcein-AM/PI, BB-4126-2) was obtained from Shanghai BestBio Science & Technology Co., Ltd (Shanghai, China). Fetal bovine serum (FBS, 10 099-141) and trypsin-EDTA (25 200-056) were acquired from Gibco, USA.

2.2. Preparation of GO-SIS biocomposite films

GO-SIS biocomposite films were prepared by using an automatic coating machine (MRX-TM300, Shenzhen Mingruixiang Automation Equipment Co., Ltd, China). The process is schematically illustrated in Fig. 1. Prior to coating, the as-received GO dispersion was diluted with deionized water to achieve a working concentration of 0.5 mg mL^{-1} and ultrasonicated for 30 minutes. The resulting stable, homogeneous dispersion showed no visible sedimentation for at least 24 h. First, a single-layer SIS film was removed from its sterile packaging and laid flat directly on a glass plate. Then, the 0.5 mg mL^{-1} GO dispersion was dropped onto the SIS film and spread using a scraper with a gap of 150 μm at a speed of 10 mm s^{-1}. After coating, the GO-SIS biocomposite films were dried in a vacuum drying oven (DZF-6020, Sobo Instrument Equipment Co., Ltd, China) at 25 °C for 8 h. The resulting GO loading on the composite films was approximately 0.05 mg cm^{-2} (SI, Table S1). Finally, the dried films were cut into desired shapes and sterilized with ethylene oxide for subsequent experiments.

2.3. Structural characterization of GO, SIS and GO-SIS biocomposite films

2.3.1 X-ray diffraction analysis. X-ray diffraction (XRD) patterns were obtained using a powder X-ray diffractometer (X-Pert3 Powder, PANalytical, the Netherlands) with Cu Kα radiation (λ = 1.54 Å). The scan range was from 5° to 60° (2θ) with a scan rate of 4° min^{-1}.

2.3.2 Fourier transform infrared spectroscopy-attenuated total reflectance analysis. Fourier transform infrared spectroscopy-attenuated total reflectance (FTIR-ATR) spectra were recorded using a Fourier transform infrared spectrometer (Nicolet iS50, Thermo Fisher Scientific, USA). The FTIR-ATR spectra were collected in the range of 400–4000 cm^{-1} with a resolution of 4 cm^{-1}.

2.3.3 Raman spectroscopic analysis. Raman spectra were acquired using a Micro Raman imaging spectrometer (DXRxi, Thermo Fisher Scientific, USA), with an excitation wavelength of 532 nm and a laser power of 1.5 mW. The scanning range was set from 200 to 3400 cm^{-1}.

2.3.4 Atomic force microscopy analysis. The atomic force microscopy (AFM) images were acquired using a Dimension Icon atomic force microscope (Bruker, Germany). The GO dispersion was diluted to near-colorlessness and then deposited onto a freshly cleaved mica substrate. Measurements were performed in tapping mode.

2.3.5 Morphological analysis. The morphology of the SIS and GO-SIS biocomposite films was observed using a field emission environmental scanning electron microscope (Quattro ESEM, Thermo Fisher Scientific, USA). The films were cut into 5 mm × 5 mm pieces, mounted on the sample stage with

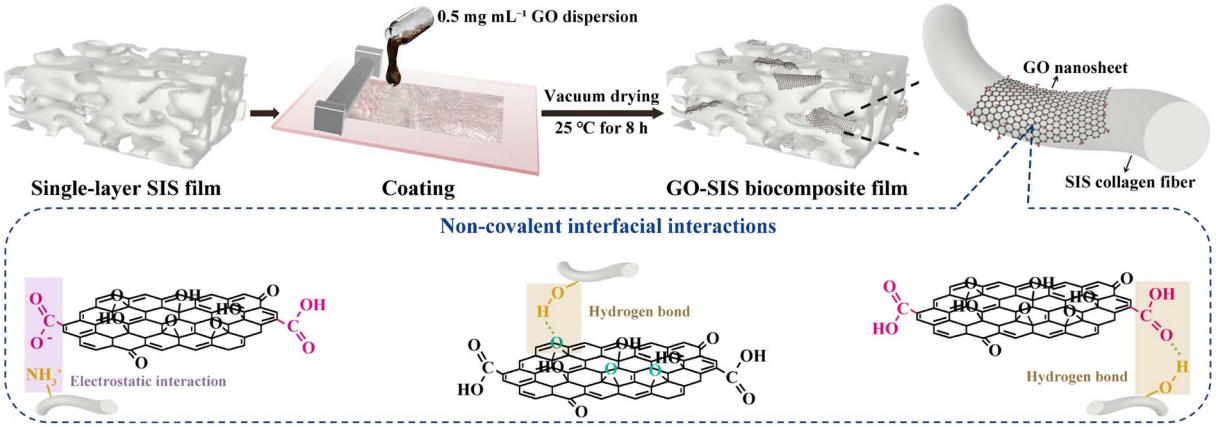

Fig. 1 Schematic of the fabrication process and non-covalent interfacial interactions in the GO-SIS biocomposite film.

conductive adhesive, and then placed into the ESEM for observation.

The thickness of the SIS and GO-SIS biocomposite films was measured using a digital micrometer (DL321025B, Deli, China, ±2 μm error). Measurements were taken at 20 random points on each of five independent films (5 cm × 15 cm), yielding 100 data points from which the average and standard deviation were calculated.

2.4. Performance characterization of SIS and GO-SIS biocomposite films

2.4.1 Contact angle measurement. The contact angles of the SIS and GO-SIS biocomposite films were measured using an optical contact angle measuring instrument (DSA30, KRUSS, Germany). The films were placed flat in the center of the sample holder. The contact angles were determined by dropping 5 μL deionized water onto the films surface at a rate of 0.5 mL min^{-1}. Five independent measurements were taken for each type of film.

2.4.2 Water absorption test. The water absorption of the SIS and GO-SIS biocomposite films was analyzed by immersing them in PBS for 24 h. First, the dry films weight (W_{dry}) was recorded. After 24 h immersion, the wet films weight (W_{wet}) was immediately measured after removing excess water. Five independent measurements were tested for each type of film. The water uptake capacity was calculated using the following equation:

$$\text{Water absorption}(\%) = \frac{W_{wet} - W_{dry}}{W_{dry}} \times 100\% \quad (1)$$

2.4.3 Mechanical properties test. The mechanical properties of the SIS and GO-SIS biocomposite films were evaluated using a microcomputer-controlled electronic universal testing machine (UTM2503X, Shenzhen Sansi Zongheng Technology Co., Ltd, China) equipped with a 200 N load cell. The tests were conducted with an initial gauge length of 5 cm at a loading rate of 10 mm min^{-1}. Prior to testing, the films were cut into rectangular strips measuring 1 cm × 7 cm. The mechanical properties were measured under both dry and wet conditions. For the wet state measurements, the strips were immersed in PBS (pH 7.4) at room temperature for 24 h. After immersion, the excess surface water was removed, and the tensile tests were performed immediately. The obtained results included stress–strain curves, tensile strength, and elongation at break. Five repeated measurements were performed for each type of film under each condition.

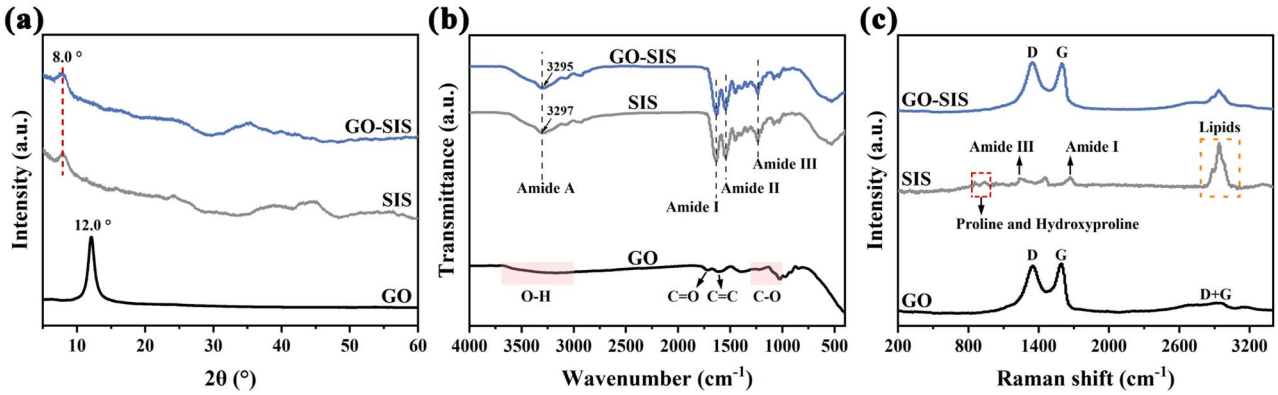

Fig. 2 Characterization of GO, SIS, and GO-SIS biocomposite films. (a) XRD patterns, (b) FTIR-ATR spectra, and (c) Raman spectra.

Table 1 Raman data of GO and the GO-SIS biocomposite film

	D band		G band		
Sample	Raman shift (cm^{-1})	FWHM (cm^{-1})[a]	Raman shift (cm^{-1})	FWHM (cm^{-1})	I_D/I_G
GO	1349	151	1584	79	0.97
GO-SIS	1349	154	1591	79	1.07

[a] FWHM, full width at half maximum.

2.4.4 *In Vitro* degradation. The weight loss rate, hydroxyproline (Hyp) content in the degradation solution, and post-degradation mechanical properties were obtained through *in vitro* degradation experiments.

In vitro degradation experiment: the experimental procedure was conducted with reference to established methods for collagen-based biomaterials.[8,37] SIS and GO-SIS biocomposite films were cut into 1 cm × 7 cm rectangular strips. The initial dry weight of each film (W_1) was measured. The films were then immersed in a 0.05 mg mL^{-1} type I collagenase solution (prepared in 0.01 M PBS, pH 7.4) at 37 °C with shaking at 200 rpm to simulate physiological collagen degradation. Predetermined time points (4, 8, 16, 24, 48, 72, 96, and 120 h) were selected to cover the complete degradation process. At each time point, the degradation solution was collected and the films were removed, dried, and weighed (W_2). For the longer incubation periods (48, 72, 96, and 120 h), the degradation solution was collected daily when the enzyme solution was refreshed. Photographs were taken at each time point. All experiments were performed in triplicate for each time point. The dried films after degradation were retained for subsequent ESEM observation and mechanical properties testing.

The weight loss rates of the films were calculated using the following equation:

$$\text{Weight loss rate}(\%) = \frac{W_1 - W_2}{W_1} \times 100\% \quad (2)$$

Hyp content determination: the Hyp content in the degradation solutions at each time point was determined according to the instructions of the Hydroxyproline assay kit. The absorbance for hydroxyproline determination (Abs_{Hyp}) was measured at 560 nm using a multifunctional microplate reader (EnSpire, PerkinElmer, USA). A standard curve was plotted using gradient concentrations of Hyp standard solution (SI Table S2 and Fig. S1). The Hyp content in the degradation solution at each time point was calculated using the following equation:

$$\text{Hyp content} = n \times V \times \frac{Abs_{Hyp} - 0.106}{0.0143} \quad (3)$$

where n is the dilution factor, and V is the degradation solution volume. For the 48 h, 72 h, 96 h, and 120 h time points, the Hyp content was calculated by summing each 24 h period.

2.4.5 Cytocompatibility evaluation. The SIS and GO-SIS biocomposite films were immersed in the culture medium (iCell-m026-001b) at a surface area to volume ratio of 6 cm^2 mL^{-1} and incubated at 37 °C for 24 h to obtain the corresponding extract solutions. The *in vitro* cytocompatibility assessment included live/dead staining and cell proliferation assays.[8,9]

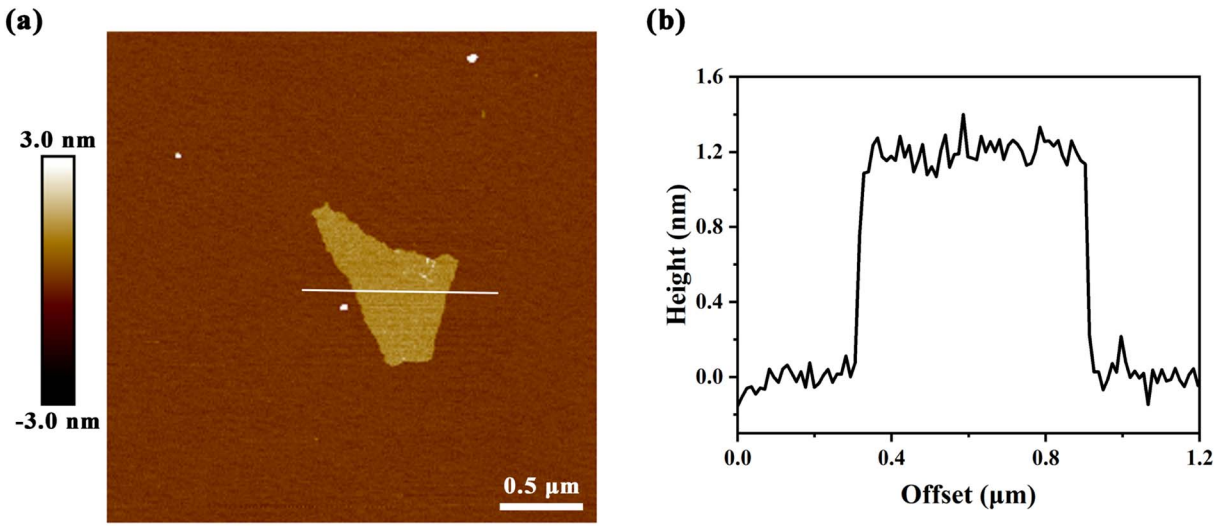

Fig. 3 (a) AFM image and (b) corresponding height profile of a GO nanosheet.

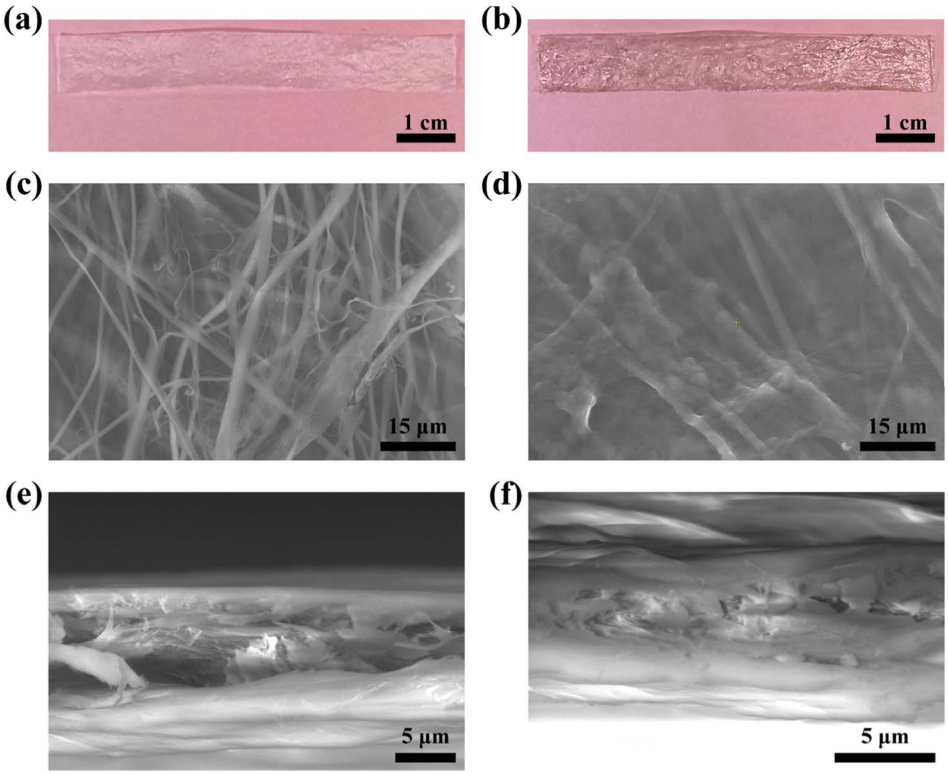

Fig. 4 Morphology of SIS and GO-SIS biocomposite films. Digital photographs of (a) SIS and (b) GO-SIS biocomposite film. Surface ESEM images of (c) SIS and (d) GO-SIS biocomposite film. Cross-sectional ESEM images of (e) SIS and (f) GO-SIS biocomposite film.

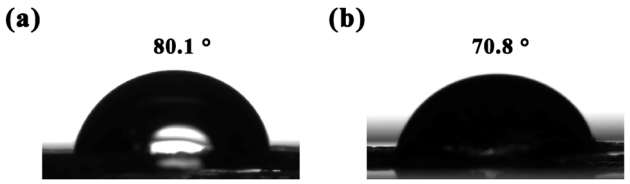

Fig. 5 Representative contact angle images of (a) SIS and (b) GO-SIS biocomposite films.

Table 2 Contact angle and water absorption data of SIS and GO-SIS biocomposite films

Sample	Contact angle (°)	Water absorption (%)
SIS	79.9 ± 2.4	140.62 ± 7.27
GO-SIS	71.3 ± 1.0	159.00 ± 5.60

Live/Dead staining assay: L929 fibroblasts (iCell-m026) were seeded in confocal dishes at a density of 5×10^4 cells per dish and cultured overnight under standard conditions (37 °C, 5% CO_2). The original culture medium was then aspirated. Cells in the control group were replenished with fresh culture medium (iCell-m026-001b), while those in the experimental groups were treated with the corresponding material extract solutions. All groups were then subjected to further incubation. A staining solution was prepared according to the instructions of the live/dead double staining kit (Calcein-AM/PI). After 1, 3, and 7 days of culture, the medium was removed, and the cells were washed twice with PBS. Subsequently, 200 μL of the staining solution was added to each dish, and the cells were incubated in the dark at 4 °C for 15–20 minutes. The stained cells were observed using a confocal microscope (TCS SP8, Leica, Germany), where live and dead cells were stained green and red, respectively.

Cell proliferation assay: L929 fibroblasts (iCell-m026) were seeded in 96-well plates at a density of 1×10^4 cells per well and cultured overnight under standard conditions (37 °C, 5% CO_2). The original medium was then aspirated. Cells in the control group were replenished with 200 μL of fresh culture medium, while cells in the experimental groups were treated with 200 μL of the corresponding material extract solutions. All experimental conditions were performed in triplicate. After 1, 3, and 7 days of incubation, the medium was removed, and the wells were washed three times with PBS. Following this, 100 μL of medium containing 10% CCK-8 reagent was added to each well, and the plates were incubated for 1-2 hours at 37 °C. The absorbance at 450 nm was measured using a microplate reader (Epoch2, BioTek, USA) to assess cell proliferation.

2.4.6 Hemolysis assay. The erythrocyte compatibility of the SIS and GO-SIS biocomposite films was assessed by a direct contact hemolysis assay using film pieces (1.5 cm × 2 cm) cut from each material. Blood was drawn from a healthy anonymous human volunteer. Erythrocytes were isolated by centrifuging the blood at 1000 rpm for 10 min, followed by washing and dilution with 0.9% NaCl solution to prepare a red blood cell

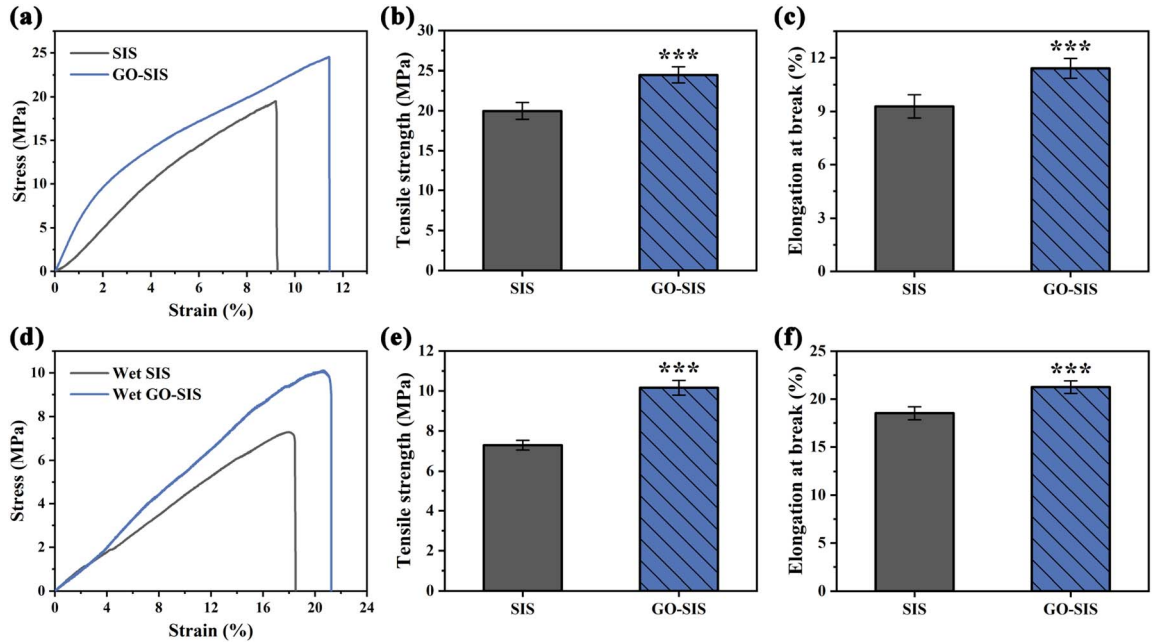

Fig. 6 Mechanical properties of SIS and GO-SIS biocomposite films. (a) Representative stress–strain curves, (b) tensile strength, and (c) elongation at break in the dry state. (d) Representative stress–strain curves, (e) tensile strength, and (f) elongation at break in the wet state. Data are presented as mean ± standard deviation (SD), $n = 5$, ***$p < 0.001$.

Table 3 Mechanical properties of SIS and GO-SIS biocomposite films

	Tensile strength (MPa)		Elongation at break (%)	
Sample	Dry	Wet	Dry	Wet
SIS	19.97 ± 1.06	7.28 ± 0.24	9.28 ± 0.66	18.53 ± 0.67
GO-SIS	24.46 ± 0.99	10.16 ± 0.37	11.41 ± 0.55	21.26 ± 0.65

(RBC) suspension for subsequent use. For the experimental groups, each film sample was placed into a 1.5 mL centrifuge tube containing 1 mL of PBS and equilibrated at 37 °C for 30 min. Subsequently, 20 μL of the RBC suspension was added to each tube. For controls, 20 μL of the RBC suspension was added to 1 mL of PBS (negative control) or to 1 mL of deionized water (positive control) in the absence of any film sample. All tubes (samples and controls) were then incubated with rotation at 37 °C for 1 h. After incubation, all mixtures were centrifuged at 3000 rpm for 5 min. Then, 200 μL of each supernatant was transferred to a 96-well plate, and the absorbance at 545 nm was measured using a multifunction microplate reader (Varioskan Flash, Thermo Fisher Scientific, USA). All samples and controls were tested in triplicate. The hemolysis rate was calculated using the following equation:

$$\text{Hemolysis rate } (\%) = \frac{\text{Abs}_t - \text{Abs}_{nc}}{\text{Abs}_{pc} - \text{Abs}_{nc}} \times 100\% \quad (4)$$

where Abs_t, Abs_{nc}, and Abs_{pc}, represent the absorbance of the test sample, negative control, and positive control, respectively.

2.5. Statistical analysis

All statistical analyses were performed using Origin 2021 software (OriginLab Corporation, USA). Data were expressed as mean ± standard deviation (SD). Normality (Shapiro–Wilk test) and homogeneity of variances (Levene's test) were verified prior to parametric testing. For data meeting these assumptions, two-group comparisons used the independent samples *t*-test, and multi-group comparisons used one-way analysis of variance (ANOVA) with Tukey's post-hoc test. Otherwise, the non-parametric Mann–Whitney test (two groups) or Kruskal–Wallis test with Dunn's post-hoc test (multi-group) was applied. Statistical significance was denoted as *$p < 0.05$, **$p < 0.01$, and ***$p < 0.001$.

3. Results and discussion

3.1. Structural characterization of GO, SIS and GO-SIS biocomposite films

3.1.1 XRD analysis. The XRD patterns of GO, SIS and GO-SIS biocomposite films are shown in Fig. 2a. It is well known that the interlayer spacing of graphite is 0.34 nm.[38] In contrast, a characteristic (001) diffraction peak for GO was observed at $2\theta = 12.0°$, corresponding to an interlayer spacing of 0.74 nm. The increased interlayer spacing resulted from the introduction of oxygen-containing functional groups.[39]

The collagen fibers of the SIS film showed a diffraction peak at $2\theta = 8.0°$, reflecting a lateral spacing of 1.10 nm between the collagen molecules.[40,41] In the GO-SIS biocomposite film, the diffraction peak of collagen fibers was observed, suggesting that coating SIS with the 0.5 mg mL^{-1} GO dispersion did not disrupt the collagen molecular structures. However, no distinct GO

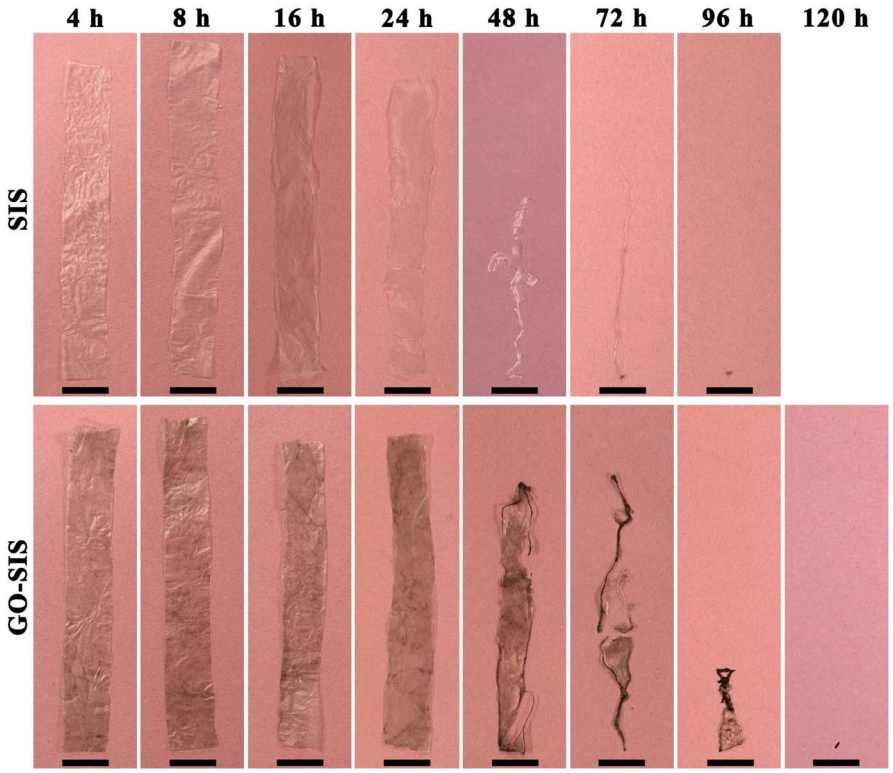

Fig. 7 Representative digital photographs of SIS and GO-SIS biocomposite films after different periods of *in vitro* degradation. Scale bars: 1 cm.

diffraction peak was detected in the GO-SIS biocomposite film, which could be attributed to the low concentration and good dispersion of GO.

3.1.2 FTIR-ATR analysis. To identify the functional groups in GO, SIS, and GO-SIS biocomposite films, as well as the interfacial interactions between GO and the collagen fibers of SIS, FTIR-ATR analysis was performed (Fig. 2b). GO exhibited absorption peaks at 3000–3700 cm^{-1}, 1720 cm^{-1}, 1620 cm^{-1}, and 1000–1300 cm^{-1}, which were attributed to O–H, C=O, C=C, and C–O stretching vibrations, respectively.[42–44] These absorption peaks indicated that GO contained functional groups such as hydroxyl (–OH), carboxyl (–COOH), and epoxy (C–O–C) groups.

In the FTIR-ATR spectrum of the SIS film, four typical bands of collagen fibers were observed, namely amide A (3297 cm^{-1}), amide I (1632 cm^{-1}), amide II (1543 cm^{-1}), and amide III (1236 cm^{-1}). The amide A band is associated with N–H stretching vibrations.[31,34] The amide I band is associated with C=O stretching vibration.[31] The amide II band consists of N–H bending vibration and C–N stretching vibration.[45] The amide III

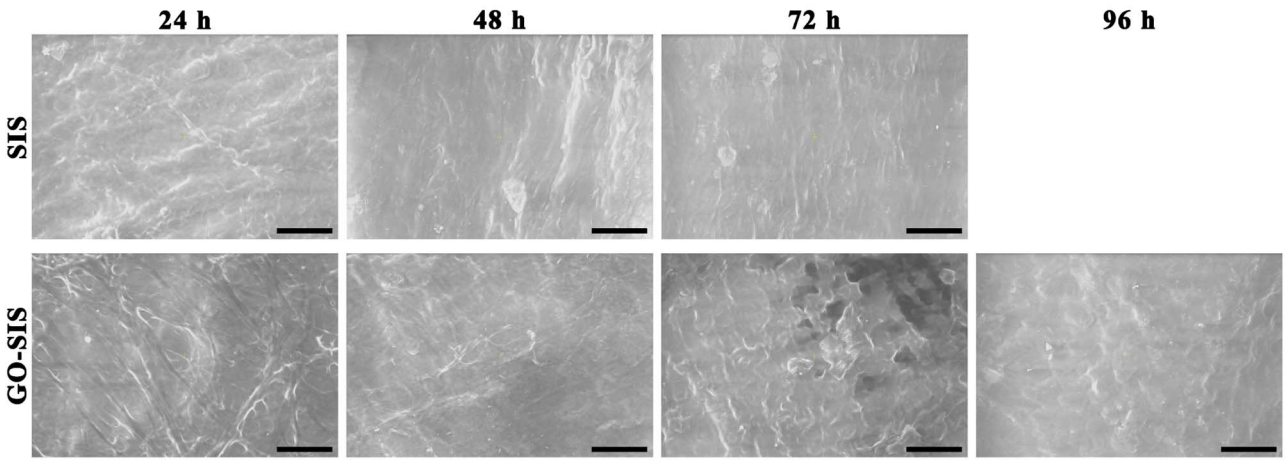

Fig. 8 Representative ESEM images showing the morphology of SIS and GO-SIS biocomposite films at key time points (24 h, 48 h, 72 h, 96 h) after *in vitro* degradation. Scale bars: 50 μm.

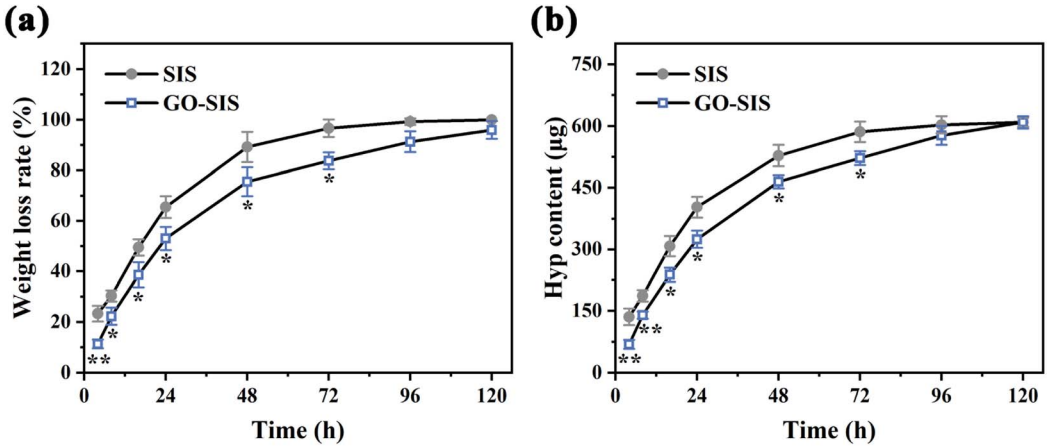

Fig. 9 Quantitative analysis of *in vitro* degradation for SIS and GO-SIS biocomposite films at different time points. (a) Weight loss rate; (b) Hyp content in the degradation solution. Data are presented as mean ± standard deviation (SD), $n = 3$, $^{*}p < 0.05$, $^{**}p < 0.01$.

band is primarily composed of C–N stretching vibration and N–H bending vibration, which is strongly influenced by the constituent amino acids.[45,46] Importantly, the amide I, II, and III bands are closely associated with the triple-helical structure of collagen molecules.[47] Therefore, these results confirm the presence of amide bonds in SIS collagen fibers. Furthermore, collagen is known to contain hydroxyl (–OH) groups, primarily derived from hydroxyproline and hydroxylysine.[48]

The FTIR-ATR spectrum of the GO-SIS biocomposite film was similar to that of the SIS film, indicating that the incorporation of GO did not change the collagen molecular structures. Compared to the SIS film spectrum, the amide A band in the GO-SIS biocomposite film exhibited a slight shift toward lower wavenumber (from 3297 cm^{-1} to 3295 cm^{-1}). This shift may be attributed to non-covalent interactions between the oxygen-containing functional groups of GO and the functional groups of SIS collagen fibers.[33,34]

3.1.3 Raman analysis. Raman spectroscopy is highly sensitive to carbon materials and is commonly used to characterize their disordered and ordered crystal structures.[49–51] In the Raman spectra of carbon materials, the disordered (D) band corresponds to the A_{1g} breathing mode, while the graphite (G) band is attributed to the first-order scattering of the E_{2g} mode.[49] The intensity ratio of the disorder-induced D band to symmetry-allowed G band (I_D/I_G) is commonly used to indicate the defect density in carbon materials.[51] It is well known that GO is one of the important carbon materials.[51] Therefore, Raman spectroscopy can be used to distinguish the structural differences between the GO-SIS biocomposite films and SIS (Fig. 2c).

In the Raman spectrum of GO, the D band at 1349 cm^{-1} and the G band at 1584 cm^{-1} were observed, with an I_D/I_G ratio of 0.97 (Table 1). Additionally, the D + G band appeared at 2911 cm^{-1}, confirming the defective and oxidized structure of the GO.[31,50,52]

The Raman spectrum of the SIS film showed characteristic features at 800–1000 cm^{-1} (proline and hydroxyproline region), 1237 cm^{-1} (Amide III band), 1669 cm^{-1} (Amide I band), and 2800–3100 cm^{-1} (lipids region), consistent with reported Raman spectra of collagen structure.[40,48]

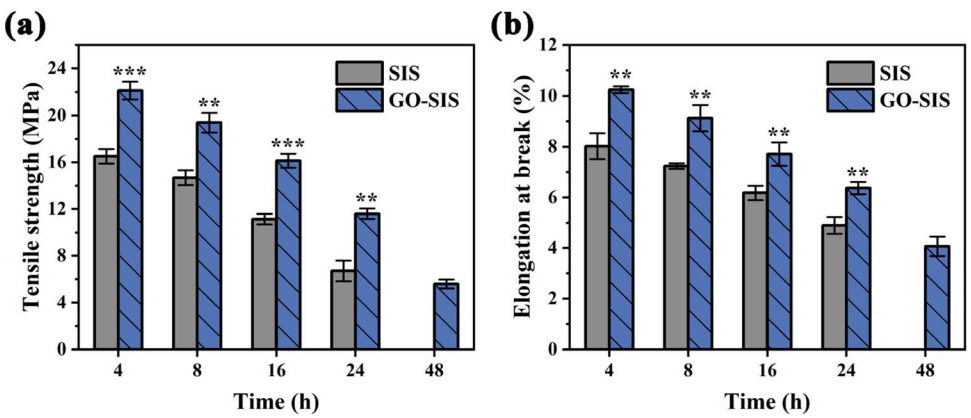

Fig. 10 Mechanical properties of dried SIS and GO-SIS biocomposite films after *in vitro* degradation. (a) Tensile strength, (b) elongation at break. Data are presented as mean ± standard deviation (SD), $n = 3$, $^{**}p < 0.01$, $^{***}p < 0.001$.

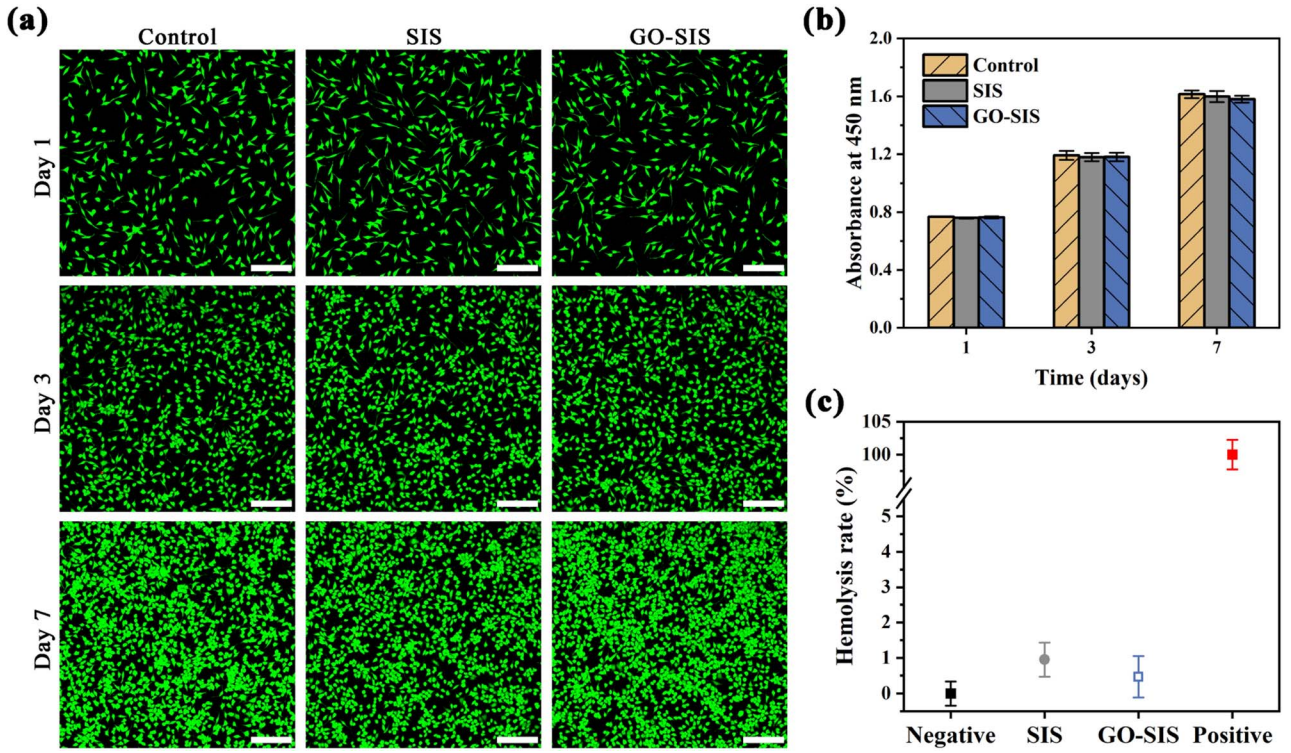

Fig. 11 Evaluation of the biocompatibility of SIS and GO-SIS biocomposite films. (a) Representative live/dead staining images of L929 fibroblasts co-cultured with extract solutions from the control, SIS, and GO-SIS groups after 1, 3, and 7 days (scale bars: 200 μm), (b) cell proliferation results of L929 fibroblasts co-cultured with the extract solutions of the control, SIS, and GO-SIS groups for 1, 3, and 7 days, and (c) hemolysis rate results.

For the GO-SIS biocomposite film, the Raman spectrum exhibited both the D and G bands corresponding to GO and the lipids region of SIS collagen fibers, confirming the successful incorporation of GO into the SIS matrix. Compared to the Raman spectrum of GO, the G band in the GO-SIS biocomposite film shifted to a higher wavenumber of 1591 cm^{-1}, and the intensity ratio of the D to G bands (I_D/I_G) increased to 1.07 (Table 1). These changes were attributed to the non-covalent interfacial interactions between the oxygen-containing functional groups of GO and the functional groups of the SIS collagen fibers,[35] which further disordered the local structure of GO nanosheets and thus enhanced the intensity of the D band.

3.1.4 AFM analysis. The morphology and thickness of the GO nanosheets were characterized by AFM. As shown in Fig. 3, the average thickness of the GO nanosheet was approximately 1.2 nm, indicating a monolayer structure. These results were consistent with previously reported studies.[52,53]

3.1.5 Morphological analysis. The morphology of the single-layer SIS and the GO-SIS biocomposite films is shown in Fig. 4. The single-layer SIS appeared as a light white translucent film (Fig. 4a), with an average thickness of 17 ± 3 μm (SI Table S3). In the ESEM images of SIS (Fig. 4c and e), a large number of collagen fibers were observed, forming a porous 3D collagen fiber structure.

In contrast, the GO-SIS biocomposite film exhibited an overall darker coloration (Fig. 4b), which is attributed to the relatively uniform addition of dark GO nanosheets to the SIS matrix. The average thickness of the GO-SIS biocomposite films was measured to be 16 ± 3 μm (SI Table S4). ESEM images of the GO-SIS biocomposite films (Fig. 4d and f) also displayed a fibrous network structure, confirming that the GO incorporation *via* the coating process did not disrupt the native collagen fiber structure of SIS. Furthermore, the collagen fibers appeared more densely interconnected compared to those in pure SIS, resulting from the coating of GO nanosheets and the non-covalent interfacial interactions between GO and SIS collagen fibers.

3.2. Performance characterization of SIS and GO-SIS biocomposite films

3.2.1 Hydrophilicity. The hydrophilicity of the SIS and GO-SIS biocomposite films was evaluated by contact angle and water absorption measurements. Representative contact angle images of SIS and GO-SIS biocomposite films are shown in Fig. 5, and the corresponding contact angle and water absorption data are summarized in Table 2. Based on these data, compared with the pure SIS film, the GO-SIS biocomposite film exhibited a significantly smaller contact angle ($p < 0.001$) and significantly higher water absorption ($p < 0.01$).

These results indicate that the non-covalent incorporation of GO significantly enhanced the hydrophilicity of the GO-SIS biocomposite film. This improvement is attributed to the ability of the abundant oxygen-containing functional groups (such as –OH and –COOH) on the GO nanosheets to form hydrogen bonds

with water,[29,54] thereby enabling the GO-SIS biocomposite film to combine with more water molecules.

3.2.2 Mechanical properties. The mechanical properties of the SIS and GO-SIS biocomposite films under both dry and wet conditions are presented in Fig. 6 and Table 3. Under dry conditions, the GO-SIS biocomposite film exhibited significantly higher tensile strength and elongation at break compared to the pure SIS film ($p < 0.001$ for both). Similarly, under wet conditions, both the tensile strength and elongation at break of the GO-SIS biocomposite film were significantly greater than those of the SIS film ($p < 0.001$).

These results indicate that the non-covalent incorporation of GO significantly enhanced the mechanical properties of the GO-SIS biocomposite film. This enhancement can be attributed to the relatively uniform incorporation of GO and the resulting non-covalent interactions (*e.g.*, electrostatic interactions and hydrogen bonding) between the abundant oxygen-containing functional groups on GO nanosheets and the functional groups on SIS collagen fibers,[12,33–35] as schematically shown in Fig. 1. These non-covalent interactions establish a robust interface between the GO nanosheets and the collagen fibers. When the GO-SIS biocomposite film is subjected to load, this interface effectively transfers and distributes stress from the SIS matrix to the high-strength GO nanosheets, thereby markedly improving the mechanical properties of the composite.[34,54] Furthermore, this efficient stress distribution helps delay premature failure caused by local stress concentration, which contributes positively to maintaining the ductility of the composite material.[33,34]

It is well recognized that the GO content and its dispersion state within the matrix are pivotal parameters governing the ultimate mechanical performance balance of GO-based composites.[12,13,55–57] Therefore, future work will involve fabricating and testing a series of GO-SIS biocomposite films through systematic variation of these parameters, aiming to define the optimal processing window.

3.2.3 *In vitro* degradation. Biodegradability is a critical functional parameter of biomaterials. The *in vitro* degradation of the SIS and GO-SIS biocomposite films was investigated using collagenase type I. Representative digital images of the SIS and GO-SIS biocomposite films at different degradation time points are presented in Fig. 7. As the *in vitro* degradation time increased, both the SIS and GO-SIS biocomposite films gradually lost their original strip-like morphology and underwent extensive degradation. After 48 hours of degradation, obvious morphological changes were observed in both the SIS film and the GO-SIS biocomposite film. Notably, the SIS film could no longer maintain their original strip-like shape, while the GO-SIS biocomposite film retained a relatively distinct strip-like morphology. By 72 hours, the SIS film had degraded into a thread-like segment, while the GO-SIS biocomposite film could no longer maintain a discernible strip morphology. By 96 hours, the SIS film was almost completely degraded, whereas the GO-SIS biocomposite film persisted as fragments. The degradation process was complete by 120 hours, with the SIS film fully degraded and only minimal residues remaining from the GO-SIS biocomposite film.

To further investigate the morphological changes of the SIS and GO-SIS biocomposite films after *in vitro* degradation, ESEM analysis was performed. As shown in Fig. 8, the collagen fiber networks in both films were progressively degraded over time. After 24 hours of degradation, the interwoven fibrous network in the SIS film had become indistinct, while the GO-SIS biocomposite film retained clearly discernible fibrous networks. By 48 hours, the surface of the SIS film had become slightly flattened, whereas the interwoven fibrous network in the GO-SIS biocomposite film had become less distinct. As the enzymatic degradation proceeded, the fibrous network of the GO-SIS biocomposite film appeared partially disintegrated and shortened by 72 hours, leading to a relatively flattened surface by 96 hours.

We also conducted a quantitative analysis of the *in vitro* degradation of the SIS and GO-SIS biocomposite films (Fig. 9). As shown in Fig. 9a, the weight loss rates of both SIS and GO-SIS biocomposite films increased over time during the degradation process. At 4, 8, 16, 24, 48, and 72 hours, the weight loss rate of the GO-SIS biocomposite film was significantly lower than that of the SIS film. Moreover, the SIS film was completely degraded after 120 hours.

Hydroxyproline (Hyp), a characteristic amino acid of collagen, is commonly used to assess the collagen content in collagen-based materials.[58] Therefore, we measured the Hyp content in the degradation solution to quantitatively evaluate the extent of collagen fiber degradation in the SIS and GO-SIS biocomposite films. As shown in Fig. 9b, during the *in vitro* degradation process, the Hyp content in the degradation solution of both SIS and GO-SIS biocomposite films showed an increasing trend over time. At 4, 8, 16, 24, 48, and 72 hours, the Hyp content in the degradation solution of the GO-SIS biocomposite film was significantly lower than that of the SIS film.

By integrating the morphological changes (Fig. 7 and 8) and quantitative analysis results (Fig. 9) of both SIS and GO-SIS biocomposite films, it can be concluded that the GO-SIS biocomposite film not only showed better morphological stability but also degraded distinctly slower *in vitro* compared to the SIS film. This indicates that the non-covalent incorporation of GO effectively delayed the degradation of the GO-SIS biocomposite film. This effect can be attributed to the GO nanosheets, which coat the collagen fibers of SIS through non-covalent interfacial interactions such as electrostatic interactions and hydrogen bonding (Fig. 1). This coating forms a barrier between collagenase and the collagen fibers, potentially obscuring or altering the enzyme cleavage sites on the collagen.[59] Consequently, this inhibits the enzyme–substrate interaction and ultimately retards the enzymatic degradation process.

To further evaluate the biodegradation performance, the mechanical properties of the dry SIS and GO-SIS biocomposite films after degradation were measured. The representative stress–strain curves of the degraded dry SIS and GO-SIS biocomposite films are shown in Fig. S2 (SI). Their tensile strength and elongation at break are shown in Fig. 10a and b, respectively. As the degradation time increased, the tensile strength of both the dry SIS and GO-SIS biocomposite films gradually decreased. At 4, 8, 16, and 24 hours, the tensile

strength of the dry GO-SIS biocomposite film was significantly higher than that of the dry SIS film. Similarly, the elongation at break of both the dry SIS and GO-SIS biocomposite films also decreased progressively with longer degradation time. At the same time points (4, 8, 16, and 24 hours), the elongation at break of the dry GO-SIS biocomposite film was significantly higher than that of the dry SIS film. After 48 hours of degradation, the pure SIS films could no longer undergo valid mechanical testing due to extensive degradation, whereas the GO-SIS biocomposite films retained measurable mechanical properties.

These results demonstrate that the GO-SIS biocomposite film exhibits better mechanical properties after *in vitro* degradation compared to the pure SIS film. The observed enhancement is attributed to the incorporation of high-strength GO nanosheets and the non-covalent interfacial interactions between GO and the SIS collagen fibers. These factors collectively facilitate load transfer and stress distribution, thereby reinforcing the mechanical properties, while concurrently forming a protective barrier around the collagen fibers to retard the enzymatic degradation process. Consequently, the better mechanical performance of the GO-SIS biocomposite film after degradation establishes a foundation for its future evaluation in dynamic physiological environments.

3.2.4 Biocompatibility. Biocompatibility is also a key functional parameter for biomaterials.[60] Live/Dead staining images (Fig. 11a) showed that nearly all cells remained viable, indicating no obvious cytotoxicity of the SIS and GO-SIS biocomposite film. Cell proliferation results (Fig. 11b) revealed that L929 fibroblasts in all groups maintained a proliferative state, with no significant differences observed among the SIS, GO-SIS, and control groups ($p > 0.05$). These results confirm the favorable cytocompatibility of the GO-SIS biocomposite film, indicating no impact on the viability and proliferation of L929 fibroblasts. Hemolysis assay results are presented in Fig. 11c. The average hemolysis rates for both the SIS and GO-SIS biocomposite films were below 5%, indicating excellent erythrocyte compatibility.

In summary, the GO-SIS biocomposite film demonstrated favorable *in vitro* biocompatibility comparable to that of pure SIS. These *in vitro* assessments lay an essential safety foundation for the further development of the GO-SIS biocomposite film. To comprehensively evaluate its potential for tissue repair, future animal studies are warranted. These will elucidate the material's performance in a complex physiological environment, focusing on long-term safety, the dynamic evolution of biomechanical properties, and effects on inflammation and ECM remodeling.

4. Conclusion

In this study, a novel GO-SIS biocomposite film was successfully developed. The introduction of GO *via* non-covalent interactions (*e.g.*, electrostatic interactions and hydrogen bonding) demonstrated favorable modification effects on SIS. Compared to the pure SIS film, the GO-SIS biocomposite film exhibited enhanced hydrophilicity, improved mechanical properties under both dry and wet conditions, and slower *in vitro* degradation. After *in vitro* degradation, the GO-SIS biocomposite film exhibited better morphological stability and mechanical properties than the SIS film. Furthermore, the GO-SIS biocomposite film had no impact on the viability or proliferation of L929 fibroblasts. Therefore, the GO-based non-covalent coating strategy proposed here offers a promising approach for developing high-performance tissue repair patches while preserving the inherent advantages of SIS. Future work will involve systematically varying the GO content and dispersion state, conducting comprehensive characterization and *in vivo* studies, to identify the optimal and rational processing parameters for enhanced clinical translation potential.

Author contributions

Mianshu Hu: writing – original draft, data curation, formal analysis, investigation, methodology, visualization. Xiuyun Chuan and Yiting Wang: writing – review & editing, conceptualization, funding acquisition, supervision. Wenyue Cheng and Kun Zhang: project administration, methodology. Yun Yan and Wenbin Zhang: resources. Jinsong Han and Jian Zhang: resources, conceptualization.

Conflicts of interest

There are no conflicts to declare.

Data availability

The data supporting the findings of this study are available within the article and its supplementary information (SI) file. Supplementary information is available. See DOI: https://doi.org/10.1039/d5ra09329e.

Acknowledgements

The authors acknowledge financial support from the National Natural Science Foundation of China (52074015 and 51774016), the Peking University Health Science Center Discipline Development Program—Clinical Medicine + X Youth Project (PKU2022LCXQ033), and the Peking University Third Hospital Fund for Interdisciplinary Research (BYSYJC2025055).

References

1 H. Capella-Monsonís, R. J. Crum, G. S. Hussey and S. F. Badylak, *Adv. Drug Deliv. Rev.*, 2024, **211**, 13.
2 S. Hinderer, S. L. Layland and K. Schenke-Layland, *Adv. Drug Deliv. Rev.*, 2016, **97**, 260–269.
3 S. F. Badylak, D. O. Freytes and T. W. Gilbert, *Acta Biomater.*, 2015, **23**, S17–S26.
4 P. Zhao, X. Li, Q. Fang, F. L. Wang, Q. Ao, X. H. Wang, X. H. Tian, H. Tong, S. L. Bai and J. Fan, *Regen. Biomater.*, 2020, **7**, 339–348.
5 L. Shi and V. Ronfard, *Int. J. Burns Trauma*, 2013, **3**, 173–179.

6 G. X. Cao, Y. Huang, K. Li, Y. B. Fan, H. Q. Xie and X. M. Li, *J. Mat. Chem. B*, 2019, **7**, 5038–5055.
7 L. Wang, W. P. Wang, J. G. Liao, F. Wang, J. Z. Jiang, C. Cao and S. R. Li, *Mater. Sci. Eng. C*, 2018, **85**, 162–169.
8 G. X. Cao, C. Y. Wang, Y. B. Fan and X. M. Li, *Mater. Sci. Eng. C*, 2020, **109**, 14.
9 F. X. Tang, D. T. Miao, R. K. Huang, B. N. Zheng, Y. Yu, P. W. Ma, B. Y. Peng, Y. Li, H. Wang and D. C. Wu, *Adv. Mater.*, 2024, **36**, 10.
10 Y. T. Wang, K. Zhang, J. F. Yang, Y. Yao, Y. Q. Guan, W. Y. Cheng, J. Zhang and J. S. Han, *Int. Urogynecol. J.*, 2023, **34**, 1501–1511.
11 K. Kim, J. Kim, S. W. Kwak, J. Y. Lee and H. Y. Kim, *Fiber. Polym.*, 2022, **23**, 2557–2564.
12 S. Tiwari, R. Patil, S. K. Dubey and P. Bahadur, *Adv. Colloid Interface Sci.*, 2020, **281**, 14.
13 Y. Zhu, S. Murali, W. Cai, X. Li, J. W. Suk, J. R. Potts and R. S. Ruoff, *Adv. Mater.*, 2010, **22**, 3906–3924.
14 J. W. Suk, R. D. Piner, J. An and R. S. Ruoff, *ACS Nano*, 2010, **4**, 6557–6564.
15 S. Ganguly, P. Das, P. P. Maity, S. Mondal, S. Ghosh, S. Dhara and N. C. Das, *J. Phys. Chem. B*, 2018, **122**, 7201–7218.
16 A. T. Smith, A. M. LaChance, S. Zeng, B. Liu and L. Sun, *Nano Mater. Sci.*, 2019, **1**, 31–47.
17 I. Jung, D. A. Field, N. J. Clark, Y. Zhu, D. Yang, R. D. Piner, S. Stankovich, D. A. Dikin, H. Geisler, C. A. Ventrice, Jr. and R. S. Ruoff, *J. Phys. Chem. C*, 2009, **113**, 18480–18486.
18 M. M. Mwaurah, J. Mathiyarasu and A. M. Vinu Mohan, *Carbohydr. Polym.*, 2025, **350**, 123060.
19 V. Georgakilas, J. N. Tiwari, K. C. Kemp, J. A. Perman, A. B. Bourlinos, K. S. Kim and R. Zboril, *Chem. Rev.*, 2016, **116**, 5464–5519.
20 C. Zhu, D. Du and Y. Lin, *2D Mater.*, 2015, **2**, 032004.
21 J. Kim, L. J. Cote, F. Kim, W. Yuan, K. R. Shull and J. X. Huang, *J. Am. Chem. Soc.*, 2010, **132**, 8180–8186.
22 H. J. Zhang, T. Yan, S. Xu, S. N. Feng, D. D. Huang, M. Fujita and X. D. Gao, *Mater. Sci. Eng. C*, 2017, **73**, 144–151.
23 H. N. Lim, N. M. Huang and C. H. Loo, *J. Non-Cryst. Solids*, 2012, **358**, 525–530.
24 J. K. Wychowaniec, J. Litowczenko and K. Tadyszak, *J. Mech. Behav. Biomed. Mater.*, 2020, **103**, 13.
25 L. Pang, C. Q. Dai, L. Bi, Z. S. Guo and J. J. Fan, *Nanoscale Res. Lett.*, 2017, **12**, 9.
26 K. L. Zhao, Y. Hao, M. Zhu and G. S. Cheng, *Acta Chim. Sin.*, 2018, **76**, 168–176.
27 R. Kurapati, J. Russier, M. A. Squillaci, E. Treossi, C. Ménard-Moyon, A. E. Del Rio-Castillo, E. Vazquez, P. Samorì, V. Palermo and A. Bianco, *Small*, 2015, **11**, 3985–3994.
28 Y. Li, L. Yang, Y. Hou, Z. Zhang, M. Chen, M. Wang, J. Liu, J. Wang, Z. Zhao, C. Xie and X. Lu, *Bioact. Mater.*, 2022, **18**, 213–227.
29 M. Heidari, S. H. Bahrami, M. Ranjbar-Mohammadi and P. B. Milan, *Mater. Sci. Eng. C*, 2019, **103**.
30 C. Y. Wan and B. Q. Chen, *Biomed. Mater.*, 2011, **6**, 8.
31 J. Cifuentes, C. Muñoz-Camargo and J. C. Cruz, *Nanomaterials*, 2022, **12**, 15.
32 H. Alimadadi, A. Yahyazadeh, A. Soltani, B. Sharifzadeh and N. O. Mahmoodi, *Res. Chem. Intermed.*, 2025, **51**, 4647–4664.
33 C. F. Yue, C. K. Ding, X. Du and B. W. Cheng, *Compos. Interfaces*, 2022, **29**, 413–429.
34 C. F. Yue, C. K. Ding, X. Du, Y. J. Wang, J. L. Su and B. W. Cheng, *Int. J. Biol. Macromol.*, 2021, **193**, 173–182.
35 A. F. Girao, G. Gonçalves, K. S. Bhangra, J. B. Phillips, J. Knowles, G. Irurueta, M. K. Singh, I. Bdkin, A. Completo and P. Marques, *RSC Adv.*, 2016, **6**, 49039–49051.
36 W. S. Hummers and R. E. Offeman, *J. Am. Chem. Soc.*, 1958, **80**, 1339.
37 F. Tang, D. Miao, R. Huang, B. Zheng, Y. Yu, P. Ma, B. Peng, Y. Li, H. Wang and D. Wu, *Adv. Mater.*, 2024, **36**, 2307845.
38 H. H. Huang, K. K. H. De Silva, G. R. A. Kumara and M. Yoshimura, *Sci. Rep.*, 2018, **8**, 9.
39 D. Liu, Q. B. Bian, Y. Li, Y. R. Wang, A. M. Xiang and H. F. Tian, *Compos. Sci. Technol.*, 2016, **129**, 146–152.
40 S. Y. Bak, S. W. Lee, C. H. Choi and H. W. Kim, *Materials*, 2018, **11**, 16.
41 E. C. Green, Y. Zhang, H. Li and M. L. Minus, *J. Mech. Behav. Biomed. Mater.*, 2017, **65**, 552–564.
42 M. Yadav, K. Y. Rhee and S. J. Park, *Carbohydr. Polym.*, 2014, **110**, 18–25.
43 X. Yan, J. Chen, J. Yang, Q. Xue and P. Miele, *ACS Appl. Mater. Interfaces*, 2010, **2**, 2521–2529.
44 S. Stankovich, R. D. Piner, S. T. Nguyen and R. S. Ruoff, *Carbon*, 2006, **44**, 3342–3347.
45 T. Riaz, R. Zeeshan, F. Zarif, K. Ilyas, N. Muhammad, S. Z. Safi, A. Rahim, S. A. A. Rizvi and I. U. Rehman, *Appl. Spectrosc. Rev.*, 2018, **53**, 703–746.
46 L. L. Fernandes, C. X. Resende, D. S. Tavares, G. A. Soares, L. O. Castro and J. M. Granjeiro, *Polímeros*, 2011, **21**, 1–6.
47 P. G. Kumar, T. Nidheesh and P. V. Suresh, *Food Res. Int.*, 2015, **76**, 804–812.
48 M. G. Martinez, A. J. Bullock, S. MacNeil and I. U. Rehman, *Appl. Spectrosc. Rev.*, 2019, **54**, 509–542.
49 D. G. Henry, I. Jarvis, G. Gillmore and M. Stephenson, *Earth-Sci. Rev.*, 2019, **198**, 102936.
50 F. H. Lyn, T. C. Peng, M. Z. Ruzniza and Z. A. N. Hanani, *Food Packag. Shelf Life*, 2019, **21**, 9.
51 R. Saito, M. Hofmann, G. Dresselhaus, A. Jorio and M. S. Dresselhaus, *Adv. Phys.*, 2011, **60**, 413–550.
52 K. Krishnamoorthy, M. Veerapandian, K. Yun and S. J. Kim, *Carbon*, 2013, **53**, 38–49.
53 H. Bai, C. Li and G. Shi, *Adv. Mater.*, 2011, **23**, 1089–1115.
54 L. Zhang, Z. P. Wang, C. Xu, Y. Li, J. P. Gao, W. Wang and Y. Liu, *J. Mater. Chem.*, 2011, **21**, 10399–10406.
55 M. Hussain, S. M. Khan, M. Shafiq, M. Al-Dossari, U. F. Alqsair, S. U. Khan and M. I. Khan, *Energy*, 2024, **308**, 132917.
56 X. Sun, C. Huang, L. Wang, L. Liang, Y. Cheng, W. Fei and Y. Li, *Adv. Mater.*, 2021, **33**, 2001105.
57 C. Liao, Y. Li and S. C. Tjong, *Int. J. Mol. Sci.*, 2018, **19**, 3564.
58 R. R. Lareu, D. I. Zeugolis, M. Abu-Rub, A. Pandit and M. Raghunath, *Acta Biomater.*, 2010, **6**, 3146–3151.
59 H. C. Liang, Y. Chang, C. K. Hsu, M. H. Lee and H. W. Sung, *Biomaterials*, 2004, **25**, 3541–3552.

60 P. Das, S. Ganguly, P. K. Marvi, M. Sherazee, S. R. Ahmed, X. Tang, S. Srinivasan and A. R. Rajabzadeh, *Adv. Funct. Mater.*, 2024, **34**, 2314520.